SLAMBOT: Structural Health Monitoring Robot using Lamb Waves

Wenyi Wang, Thomas C. Henderson, and Anshul Joshi
University of Utah

Edward Grant
North Carolina State University

UUCS-14-001

School of Computing
University of Utah
Salt Lake City, UT 84112 USA

27 May 2014

Abstract

We propose the combination of a mobile robot and a computational sensor network approach to perform structural health monitoring of structures. The robot is equipped with piezoelectric sensor actuators capable of sending and receiving ultrasound signals, and explores the surface of a structure to be monitored. A computational model of ultrasound propagation through the material is used to define two structural health monitoring methods: (1) a time reversal damage imaging (TRDI) process, and (2) a *damage range sensor (DRS)* (i.e., it provides the range to damaged areas in the structure). The damage in the structure is mapped using the DRS approach.

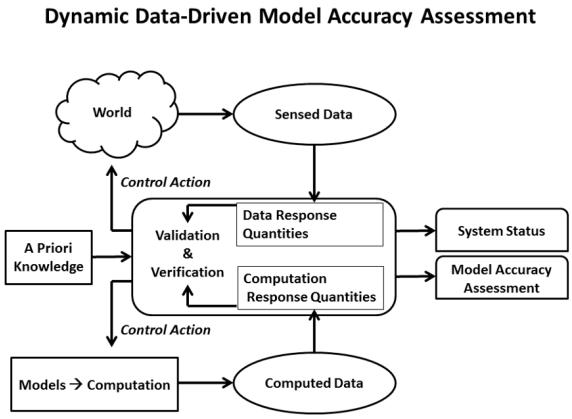

Figure 1: Verification and Validation for Bayesian Computational Sensor Networks.

1 Introduction

Periodic inspection of aircraft structures is required to determine if maintenance and repair must be performed due to damaged elements. Since down time for the aircraft is costly, uncertainty bounds are useful to making cost effective repair decisions. The Dynamic Data Driven Application System (DDDAS) approach acquires data dynamically, and compares that to a model of the structure to solve this problem. The use of Bayesian methods allows an iterative process in which the computational model is updated (e.g., Young's modulus, diffusion constants, etc.), and inverse problems can be used to improve knowledge of the sensor system and the data it produces (e.g., pose, noise, hysteresis, etc.).

Current ultrasonic sensing systems based on Lamb waves are mostly experimental (see [24] for a very good overview of this topic), and one of our goals is to develop robust methods for structural health monitoring which can then be applied even when there are uncertainties in the measurements, system models and sensor locations, as well as possible time variations of the underlying systems. The overall goal of this work is to advance the DDDAS state-of-the-art by developing a framework in which the data acquired for a specific aircraft allow the most cost effective determination of whether damage has been produced in the structure, and the location of the possible damage.

Previous work by the authors has shown how Computational Sensor Networks (CSN) [14, 13, 15, 16, 17] combine computational models of physical phenomena (e.g., heat flow, ultrasound, etc.) with sensor models to monitor and characterize a variety of systems. Our overall DDDAS approach is shown in Figure 1. This approach is based on the validation, calibration and prediction process as described by Oberkampf [21]. Experiments are used to establish parameters in the computational model, and these in turn affect the result of

the validation metric. Both simulations and physical experiments are used to help with experiment design as well as to inform the computational modeling process.

1.1 Ultrasound-based Damage Assessment

Active SHM is performed by exciting the structure to be monitored with waveforms produced by an actuating transducer. Signals propagated from each actuator are collected at sensors distributed on the structure. Assuming that we have baseline signals collected from the structure at some time, any change in the structure (for example, new damage) will result in corresponding changes in the sensor signals. Figure 2 shows an example. The bottom left panel displays the sensor signal from a healthy structure. Assuming that new damage was introduced in the structure as shown in the top right panel, we can expect new measurements using the same transducer-sensor pairs to contain reflected components of the excitation waveforms from the boundaries of the damage. The waveform depicted in the bottom right panel describes such a scenario. Based on the properties of the received signals, the damage state of the structure is estimated. In the example of Figure 2, one may estimate the time of arrival of the directly propagated waveform and the reflected component. Knowing the velocity of propagation (we assume in this example that the structure is isotropic), we can define an ellipse on which the reflecting boundary lies. This is shown in Figure 3. With the help of multiple actuator-sensor pairs, we may then estimate the boundary of the anomaly in the structure. Other methods for locating the damage and characterizing the extent of the damage are also available.

These algorithms are implemented so that automated monitoring of the structure may be achieved. An alternate approach to bonding or embedding sensors on the structure is to employ mobile robotic elements to sense at selected locations on the structure. Such a technique is under study in our research. Knowledge of the input wave, time difference between transmission and reception of different components in the sensor waveform, as well as the wave propagation properties of the structure, taken together allow the estimation of damage existence, location and scale.

The basics of robot sensing for structural health monitoring is as follows. A picture of a robot equipped with two sensors used in this work is shown in Figure 14. The robot has two ultrasound transducers fixed at a distance L apart as shown in the figure. A set of samples are taken over the surface of the structure, and assuming that parameters characterizing the undamaged structure are available, a baseline model of the sensor signal for each actuator-sensor pair can be estimated.

By moving the robot and obtaining several range estimates, the intersection of the ellipses

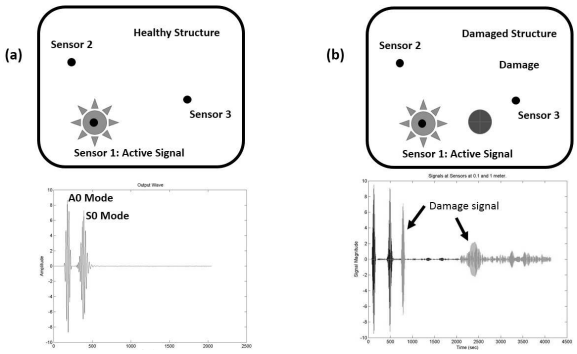

Figure 2: Ultrasound Transducer Sensor Network.

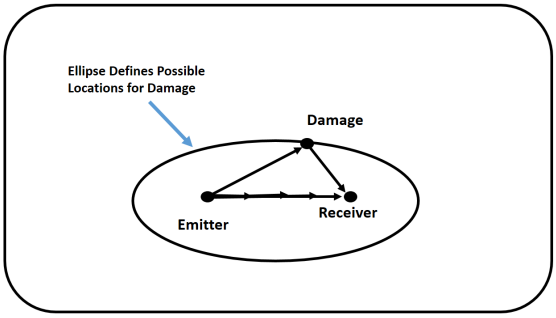

Figure 3: Damage Detection with Ultrasound Network.

provides an estimate of the damage location. By circumnavigating the detected damage location, the robot can use the range information to determine the reflecting boundaries of the damage, and thus, its extent.

2 Lamb Waves in Structural Health Monitoring

Figure 4 lays out the approach to using Lamb waves for SHM. Lamb waves are guided waves that propagate in solid structures. In active SHM systems, Lamb waves may be induced in the structure by ultrasound transducers that may act as actuators and sensors as needed. The propagation takes place in multiple modes. The velocity of each mode at any location of the structure depends on the product of the frequency of excitation and the thickness of the structure at that location. Figure 5 displays the phase velocity of different Lamb wave modes in an Aluminum plate. Because of the frequency dependent velocity profiles, the propagation of these modes is dispersive. For a detailed introduction to ultrasound waves, see [23]; there has also been a lot of work in the application of these techniques

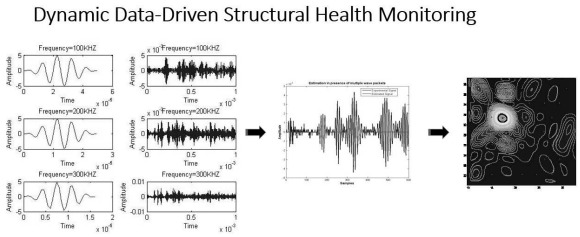

Figure 4: Lamb Wave-based Structural Health Monitoring.

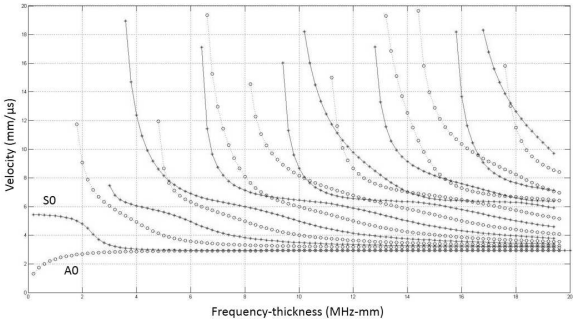

Figure 5: Lamb Wave Dispersion Curves.

in SHM (see [7, 8, 9, 10, 18, 19, 28], as well as a number of Air Force Masters theses on the topic [1, 2, 3, 5, 6, 11, 20, 22, 26]. For an excellent recent study on a data-driven approach, see [12]. Overlapped original and reflected modes (from boundaries or damaged areas) are then separated, and finally damage locations are identified based on this knowledge. Online model accuracy assessment is crucial since the multimodal and dispersive characteristics of Lamb waves may change due to changes in environmental conditions and structural properties. Such changes may result in the failure of static damage localization models, and thus in the DDDAS approach, the models are updated (re-calibrated) in every data collection step.

2.1 TRDI: Imaging in a Homogeneous Aluminum Plate Using Ultrasonic Waves

In this approach we image the cracks or other damage using the Kirchhoff migration method which exploits the waves scattered from the cracks to image them. The aluminum plate is considered sufficiently thin so that the Lamb wave approximation determines the modes that travel in the plate. No boundary effects occur since the plate is assumed infinite. First we present the Lamb approximation for the propagation of waves in a plate. At a high

level, this is described as follows: Green's function is given through $k(\omega) = \frac{\omega}{C(\omega)}$, and wave propagation is given by the convolution of the source function and Green's function. Then the imaging technique is explained, and finally numerical results are given.

Suppose each transducer emits an identical signal source. Denote the source function by f as a function a time. Assume the wave propagation satisfies Helmholtz equation:

$$\Delta u + k^2 u = 0$$

for each frequency ω, where $k = \frac{\omega}{c(\omega)}$ is a function of ω, and $c(\omega)$ is the phase velocity. Green's function is the solution of the Helmholtz equations. In the frequency domain, $\hat{G}(S, R, \omega)$ indicates the wave propagates to R if a unit point source is emitted at S at angular frequency ω. In a two-dimensional plate, $\hat{G}(S, R, \omega) = \frac{i}{4} H_0^{(1)}(k\|S - R\|)$. A signal received from source S to receiver R is given by:

$$s(S, R, t) = f(t) * G(S, R, t)$$
$$= \frac{1}{2\pi} \int_{-\infty}^{\infty} \hat{f}(\omega) \hat{G}(S, R, \omega) e^{-i\omega t} d\omega,$$

where $\hat{f}(\omega) = \int_{-\infty}^{\infty} f(t) e^{i\omega t} dt$, and $\hat{G}$ is the two point Green function at radian frequency ω.

Let D be a range of passive scatterers, which is quiet and can be detected and imaged from scattered signals received. Then using the Born approximation, the signal received from source S to D and scattered to receiver R is:

$$P(S, R, t) = \frac{1}{2\pi} \int_{-\infty}^{\infty} \hat{P}(S, R, \omega) e^{-i\omega t} d\omega,$$

where

$$\hat{P}(S, R, \omega) = k^2 \hat{f}(\omega) \int_D \rho(y) \hat{G}(S, y, \omega) \hat{G}(y, R, \omega) dy$$

with ρ the reflectivity function on D, $k = \frac{\omega}{C(\omega)}$ is the wavenumber, and $C(\omega)$ is the phase velocity at frequency ω. We model damage as passive scatterers.

Wave propagation in an aluminum plate with uniform thickness is described as Lamb waves. The central frequency $\frac{\omega_0}{2\pi}$ we use is 2×10^5 Hz. In our setup, only two Lamb wave modes need to be considered: the first anti-symmetric mode (A_0) and the first symmetric mode (S_0). We neglect the effect of all the other modes. For each mode, the Green function is $\hat{G}(A, B, \omega) = e^{-ik(\omega)\|A-B\|}$, where $k(\omega) = \frac{\omega}{C(\omega)}$ is the wave number of corresponding frequency, various in different modes. C is solved numerically based on the following equations: Let $p^2 = (\frac{\omega}{C_p})^2 - k^2$ and $q^2 = (\frac{\omega}{C_s})^2 - k^2$. For the A_0 mode,

$$\frac{tan(qh)}{tan(ph)} + \frac{4k^2 pq}{(q^2 - k^2)^2} = 0. \tag{1}$$

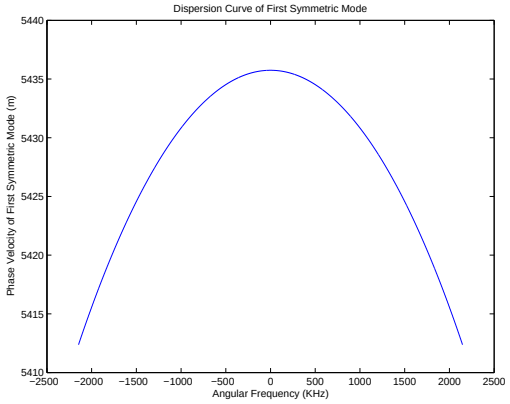

Figure 6: Dispersion Curve of First Symmetric Mode

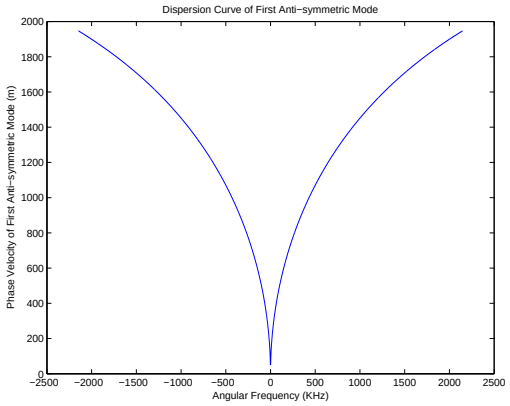

Figure 7: Dispersion Curve of First Anti-symmetric Mode

and

$$\frac{tan(qh)}{tan(ph)} + \frac{(q^2 - k^2)^2}{4k^2pq} = 0 \tag{2}$$

for the S_0 mode. C_p, C_s, and h are material constants, which are compressional wave velocity, shear wave velocity, and half plate thickness, respectively [23]. Dispersion relations for first symmetric and anti-symmetric models are shown in Figures 6 and 7 with C_p, C_s and h equal $6270m/s$, $3140m/s$ and $0.8mm$, respectively. At each angular frequency ω, corresponding phase velocities are numerical solutions of equations 1 and 2 by $fzero$ functions in **MATLAB** for $\omega > 10KHz$. Initial values for the first $\omega > 10KHz$ are given by $5500m/s$ and $1500m/s$ for the S_0 and A_0 modes, respectively. Due to the continuity of solutions with respect to ω, initial values for each ω are taken from solutions for the previous ω. Note, solutions of equations 1 and 2 are even functions. So it suffices to solve

only nonnegative frequencies. Frequencies of less than $10KHz$ are, in general, not easily solvable by the $fzero$ function. To avoid singular cases, spline interpolation is applied to those frequencies.

We are given N received signals $P_1, P_2, \ldots, P_N$ with N pairs of source and receive locations $X_{S_1}, \ldots, X_{S_N}$, and $X_{R_1}, \ldots, X_{R_N}$. The unknown reflectivity function ρ is imaged by applying time reversal techniques. The idea of time reversal is to reverse the signals $P_1, P_2, \ldots, P_N$ and back propagate them numerically. The back propagated signals in principle will focus on the scatterers with magnitude proportional to the integral of ρ on neighborhood regions.

To image the unknown reflectivity $\rho(y)$ on search point y, we evaluate P_j at deterministic arrival times

$$t_j(y,\omega) = \frac{\|X_{S_j} - y\|}{C(\omega)} + \frac{\|X_{R_j} - y\|}{C(\omega)}$$

for all $j = 1, 2, \ldots, N$ and $\omega \in \mathbb{R}$. Hence the Kirchhoff migration imaging functional [4] is given by:

$$S^{IM}(y) = \sum_{j=1}^{N} \frac{1}{2\pi} \int_{-\infty}^{\infty} \hat{P}_j(\omega) \exp(-i\omega t_j(y,\omega)) d\omega$$

Note: the imaging functional is linear with respect to received signals. This implies that is it computationally effective as an online algorithm, and suitable for dynamic data driven system.

2.1.1 Numerical Results

Here we provide numerical results of imaging an aluminum plate as modeled above. Computation that involves continuous Fourier transformations or inverse Fourier Transformations are approximated by Riemann sums by using the fast Fourier transform. We use sets of finite points as representatives of scatterer regions. Instead of integrating over scatterer regions, we sum the corresponding function at scatterer points and use the source function $f(t) = e^{i\omega_0(t-t_0)} e^{-\frac{(t-t_0)^2}{2\sigma^2}}$, where $\omega_0 = 4\pi \times 10^5, \sigma = 3 \times 10^5$, and t_0 is the signal emit time. In the following figures, red, blue and black crosses indicates source, receiver and scatterer locations, respectively. In Figures 8 to 10, we image line scatterers in $1m \times 0.4m$ windows with different modes of signals and intersection angles between path of measurements and

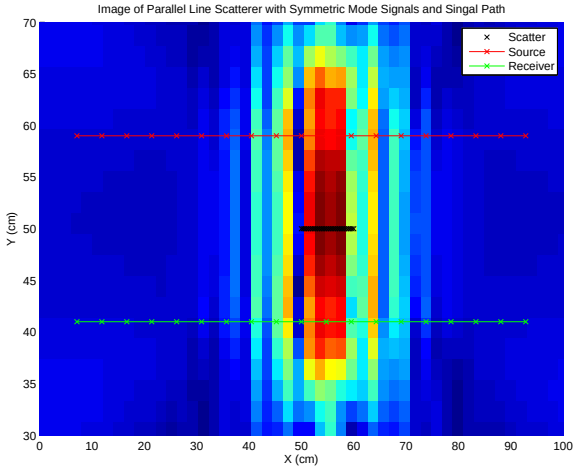

Figure 8: Image of Parallel Line Scatterer with Symmetric Mode Signals and Signal Path

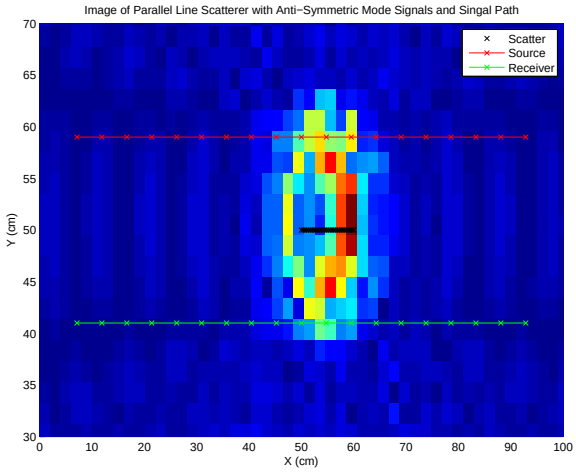

Figure 9: Image of Parallel Line Scatterer with Anti-Symmetric Mode Signals and Signal Path

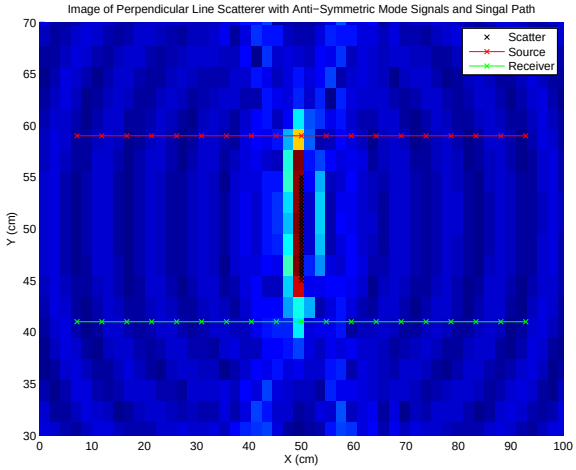

Figure 10: Image of Orthogonal Line Scatterer with Anti-Symmetric Mode Signals and Signal Path

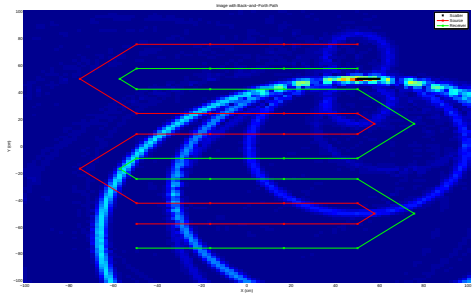

Figure 11: Image with Back−and−Forth Path

scatterer. By comparing 8 and 9 we see that imaging with Anti-symmetric mode signals has higher resolution. Figures 9 and 10 shows that making measurements orthogonal to the line scatter helps resolution. The following images are done by processing Anti-symmetric mode signals. Figures 11 to 13 show images in scenarios such that a robot is carrying sensors, moving, and making 25 measurements in $2m \times 2m$ plate. Robot paths in Figures 11 to 12 were pre-designed with certain patterns. It was found experimentally that measurements often exhibit artifacts, but that the path generated by a simple symmetric random walk as shown in Figure 13 has less artifacts in general.

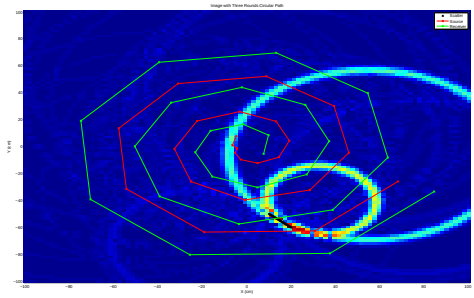

Figure 12: Image with Three Rounds Circular Path

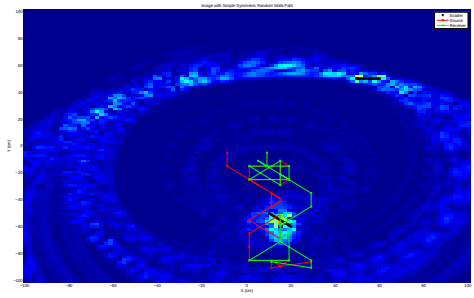

Figure 13: Image with Random Walk Paths

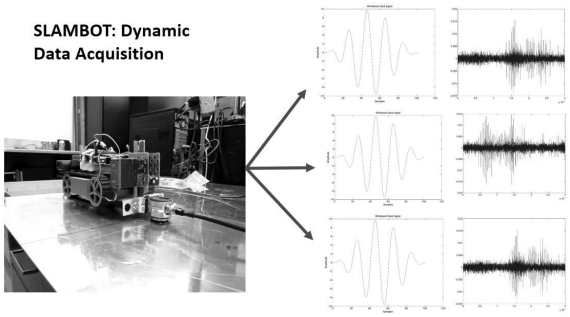

Figure 14: SLAMBOT for Dynamic Data Acquisition. The SLAMBOT is shown on the left; on the right, the structure is excited in three different locations, and the final column is the received signal for each; note that the reflected damage signal can be seen trailing the direct signal.

2.2 SLAMBOT: Simultaneous Localization and Mapping using Lamb Waves

We are currently developing a mobile robot platform which can move around on a structure to take data (see Figure 14). Based on a modified Systronix *Trackbot* mobile platform, the SLAMBOT has two attached actuation systems which cause the robot to be lifted off the surface when the ultrasound sensors are used, thus, reducing the interference from the robot on the sensor signals. Our current work is on Simultaneous Localization and Mapping (SLAM) using Lamb waves (see [25] for a detailed account of the SLAM methodology). The damage (and boundary) locations are considered point landmarks since the reflected signal returned from the closest reflecting point determines the range value. The range calculation method described earlier (shown in principle in Figure 3) is used by finding the arrival time of the second Lamb wave signal received (the first being from the straight line path from the transducer). The total number of features is controlled by the data acquisition process, and both the range data and the robot motion are assumed to have been corrupted by additive Gaussian noise.

Because we only use positive landmark detection (landmarks that show up in the range data as opposed to those occluded by other objects), as well as the conditions given above, EKF SLAM works in this setting (see [25]). We therefore estimate the robot pose $s_t = (x, y, \theta)$ as well as the landmark locations $(F_i = f_{i,x} f_{i,y} f_{i,s})$ $i = 1 \ldots n$, simultaneously using a combined state vector. Then given a motion mode for the robot:

$$p(s_t \mid u_t, s_{t-1})$$

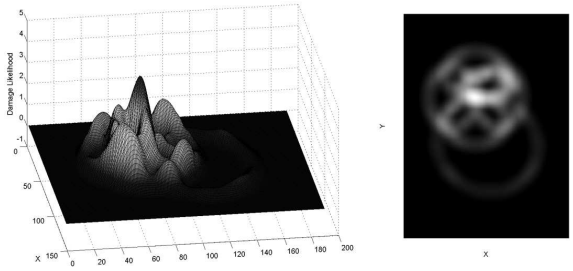

Figure 15: Simulation of Damage Localization using the Lamb Wave Range Sensor. On the left is a surface plot view of the accumulator values; on the right a 2-D image representation.

where u_t here indicates the robot control. The measurement model is:

$$p(z_t \mid s_t, F, n_t)$$

The SLAM problem is to find all landmark locations and the robot's pose using the measurements and control values; that is, the posterior:

$$p(s^t, F \mid z^t, u^t)$$

We assume feature correspondence is known, and use Algorithm *EKF SLAM known correspondences* (see Table 10.1 [25], p. 314). The results of a simulation of the Lamb wave based range finder are shown in Figure 15 (left). In this example, a 2 m X 2 m aluminum plate is used with the origin at the center (thus range in $x = [-1, 1]$ and range in $y = [-1, 1]$) with one damage location at $(-0.4, -0.4)$. The robot places the actuator and receiver at six different locations around the damage, and each range value constrains the location of the reflecting point to be on an ellipse with the actuator and receiver locations as foci. Thus, by using an accumulator array and adding a 'vote' to each location on the ellipse, these six sensed range values allow the determination of the most likely location of the reflecting point (damage in this case). This 'voting' is done with a Gaussian spread which leads to the smooth accumulator surface shown in the figure. Figure 15 (right) shows a 2-D visualization of the strength of damage location likelihood based on this data.

Figure 16 shows the experimental layout for our testing scenario. The aluminum panel was 1.6 mm thick, the sensors were VS900-RIC Vallen transducers, and the excitation signal was a 100 KHz 2.5 cycle, Hann-windowed waveform. (Note that we have not fully implemented the SLAM approach in the experimental setup, but are now able to acquire data and obtain range results.) The actuator and receiver sensors are placed as shown and a sensor reading taken for each location. Figure 17 shows five range ellipses derived from the ultrasound signals. As can be seen, the intersection of the signals localizes the damage in the structure (in this case a hole in an aluminum plate). Figure 18 shows observed signals and simulated reflected A0 mode signals with known minimized possible

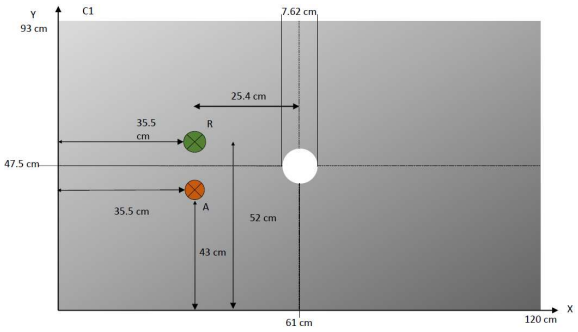

Figure 16: Experimental Layout for Damage Localization using the Lamb Wave Range Sensor in an Aluminum Plate.

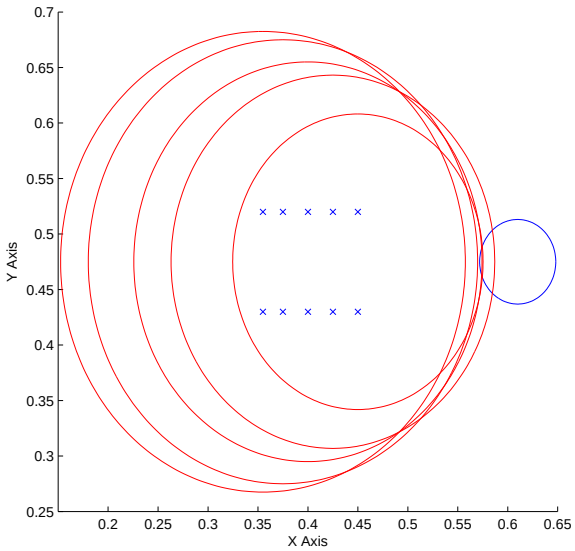

Figure 17: Ultrasound Signals received (4 locations).

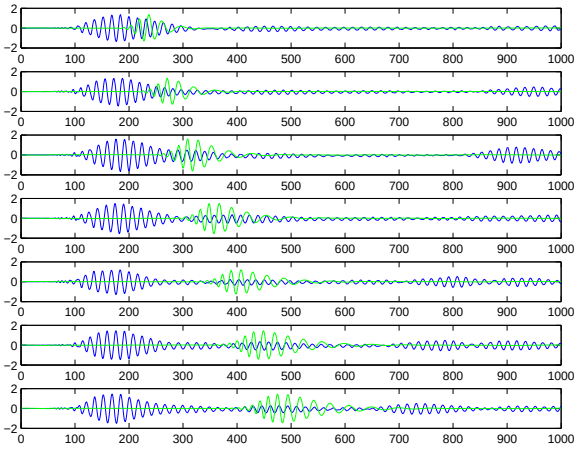

Figure 18: First Step in DSR Sensor comparing Actual Data with Simulated Signal.

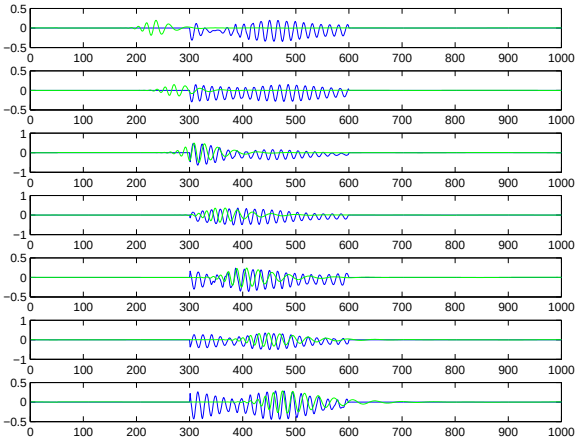

Figure 19: Windowed SAP Signal versus Simulated Signal.

reflection range. The simulated reflected signal has much overlap with directly propagated signals in the real data in first two cases. This means there must be a good way to separate directly propagate waves (between the actuator and receiver transducers) and the reflected waves in the observed data, otherwise, data taken with a reflected distance smaller than some threshold cannot be considered. Another issue is that some of the earliest reflected signals are not the main component reflected signals in the data. To avoid these two issues, we simply window out signals outside a certain reflection range. Figure 19 shows the windowed signals versus the simulated signals as described above. In this form, the peak amplitude not clearly identifiable. We therefore compute the CWT_based scaled-average wavelet power (SAP) (see [24] page 166, for a description of this method). The computed SAPs are shown in Figure 20; in this figure, the peaks are more clearly discernible.

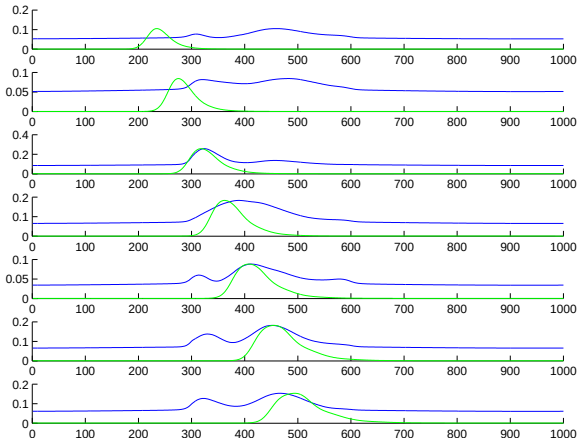

Figure 20: Computer Scaled-Average wavelet power (SAPs).

3 Conclusions and Future Work

We propose a Bayesian Computational Sensor Network approach as a formal basis for Dynamic Data Drive Application Systems. To date, we have shown that this can be effective in the 1D domain of heat flow, and we are currently working to develop a robust aircraft structural health monitoring framework based on the use of Lamb waves. A dynamic data acquisition method using a mobile robot has been described. Future work includes the experimental validation of the approach as well as a formal analysis of the uncertainty quantification. We are constructing several mobile robots and will perform experiments using single and multiple robots to map damage in plate structures. The experiments will first be performed with Aluminum plates, and then on composite structures.

We are currently exploring the field of uncertainty quantification [27] in order to provide bounds on the confidence of inferences about the behavior of the *SLAMBOT* based on computational models and sensor data. In particular, we aim to characterize the uncertainty properties of the range sensor function described earlier.

Acknowledgments: This work was supported by AFOSR-FA9550-12-1-0291. We would also like to thank our colleagues V.J. Mathews, D. Adams and F. Guevara Vasquez for helpful discussions.

References

[1] A.P. Albert, E. Antoniou, S.D. Leggiero, K.A. Tooman, and R.L. Veglio. A Systems Engineering Approach to Integrated Structural Health Monitoring for Aging Aircraft. Master's thesis, Air Force Institute of Technology, Ohio, March 2006.

[2] J.P. Andrews. Lamb Wave Propagation in Varying Thermal Environments. Master's thesis, Air Force Institute of Technology, Ohio, March 2007.

[3] M. Barker, J. Schroeder, and F. Gürbüz. Assessing Structural Health Monitoring Alternatives using a Value-Focused Thinking Model. Master's thesis, Air Force Institute of Technology, Ohio, March 2009.

[4] N. Bleistein, J.K. Cohen, and Jr John W. Stockwell. *Mathematics of Multidimensional Seismic Imaging, Migration, and Inversion*, volume 13. Springer, 2001.

[5] M.S. Bond, J. A Rodriguez, and H.T. Nguyen. A Systems Engineering Process for an Integrated Structural Health Monitoring System. Master's thesis, Air Force Institute of Technology, Ohio, March 2007.

[6] J.S. Crider. Damage Detection using Lamb Waves for Sructural Health Monitoring. Master's thesis, Air Force Institute of Technology, Ohio, March 2007.

[7] Q.-T. Deng and Z.-C. Yang. Scattering of S_0 Lamb Mode in Plate with Multiple Damage. *Journal of Applied Mathematical Modeling*, 35:550–562, 2011.

[8] V. Giurgiutiu. Tuned Lamb Wave Excitation and Detection with Piezoelectric Wafer Active Sensors for Structural Health Monitoring. *Journal of Intelligent Material Systems and Structures*, 16(4):291–305, April 2005.

[9] S. Ha and F.-K. Chang. Optimizing a Spectral Element for Modeling PZT-induced Lamb Wave Propagation in Thin Plates. *Smart Mater. Struct.*, 19(1):1–11, 2010.

[10] S. Ha, A. Mittal, K. Lonkar, and F.-K. Chang. Adhesive Layer Effects on Temperature-sensitive Lamb Waves Induced by Surface Mounted PZT Actuators. In *Proceedings of 7th International Workshop on Structural Health Monitoring*, pages 2221–2233, Stanford, CA, September 2009.

[11] S.J. Han. Finite Element Analysis of Lamb Waves acting within a Thin Aluminum Plate. Master's thesis, Air Force Institute of Technology, Ohio, September 2007.

[12] J.B. Harley and J.M.F. Moura. Sparse Recovery of the Multimodal and Dispersive Characteristics of Lamb Waves. *Journal of Acoustic Society of America*, 133(5):2732–2745, May 2013.

[13] T.C. Henderson. *Computational Sensor Networks*. Springer-Verlag, Berlin, Germany, 2009.

[14] T.C. Henderson, C. Sikorski, E. Grant, and K. Luthy. Computational Sensor Networks. In *Proceedings of the 2007 IEEE/RSJ International Conference on Intelligent Robots and Systems (IROS 2007)*, San Diego, USA, 2007.

[15] Thomas C. Henderson and Narong Boonsirisumpun. Issues Related to Parameter Estimation in Model Accuracy Assessment. In *Proceedings of the ICCS Workshop on Dynamic Data Driven Analysis Systems*, Barcelona, Spain, June 2013.

[16] Thomas C. Henderson, Kyle Luthy, and Edward Grant. Reaction-Diffusion Computation in Wireless Sensor Networks. In *Proceedings of the Workshop on Unconventional Approaches to Robotics, Automation and Control Inspired by Nature, IEEE International Conference on Robotics and Automation*, pages 13–15, Karlsruhe, Germany, May 2013.

[17] Thomas C. Henderson, Kyle Luthy, and Edward Grant. Reaction-Diffusion Computation in Wireless Sensor Networks. *Jounral of Unconventional Computing*, page to appear, 2014.

[18] B. C. Lee and W. J. Staszewski. Modelling of Lamb Waves for Damage Detection in Metallic Structures: Part I. Wave Propagation. *Smart Mater. Struct.*, 12(5):804–814, October 2003.

[19] B. C. Lee and W. J. Staszewski. Lamb Wave Propagation Modelling for Damage Detection: I. Two-dimensional Analysis. *Smart Mater. Struct.*, 16(5):249–259, 2007.

[20] E. Lindgren, J.C. Aldrin, K. Jata, B. Scholes, and J. Knopp. Ultrasonic Plate Waves for Fatigue Crack Detection in Multi-Layered Metallic Structures. Technical Report AFRL-RX-WP-TP-2008-4044, Air Force Research Laboratory, December 2008.

[21] W.L. Oberkamf and C.J. Roy. *Verification and Validation in Scientific Computing*. Cambridge University Press, Cambridge, UK, 2010.

[22] F. Ospina. An Enhanced Fuselage Ultrasound Inspection Approach for ISHM Purposes. Master's thesis, Air Force Institute of Technology, Ohio, March 2012.

[23] J. L. Rose. *Ultrasound Waves in Solid Media*. Cambridge University Press, Cambridge, UK, 1999.

[24] Z. Su and L. Ye. *Identification of Damage using Lamb Waves*. Springer Verlag, Berlin, Germany, 2009.

[25] S. Thrun, W. Burgard, and D. Fox. *Probabilistic Robotics*. MIT Press, Cambridge, MA, 2006.

[26] R.T. Underwood. Damage Detection Analysis Using Lamb Waves in Restricted Geometry for Aerospace Applications. Master's thesis, Air Force Institute of Technology, Ohio, March 2008.

[27] D. Xiu. Fast Numerical Methods for Stochastic Computations: A Review. *Communications in Computational Physics*, 5(2–4):242–272, 20109.

[28] Y. Ying, Jr. J.H. Garrett, J. Harley, I.J. Oppenheim, J. Shi, and L. Soibelman. Damage Detection in Pipes under Changing Environmental Conditions using Embedded Piezoelectric Transducers and Pattern Recognition Techniques. *Jnl of Pipeline Systems Engineering and Practice*, 4:17–23, 2013.